



On the estimation of multiaxial elastoplastic notch stresses and strains under in-phase proportional loadings



Marco Antonio Meggiolaro^{a,*}, Jaime Tupiassú Pinho de Castro^a, Luiz Fernando Martha^a,
Luiz Fernando Nazaré Marques^b

^a Pontifical Catholic University of Rio de Janeiro, PUC-Rio, Rua Marquês de São Vicente 225, Rio de Janeiro 22451-900, Brazil

^b Federal University of South and Southeast of Pará, UNIFESSPA, Avenida dos Ipês s/n, Marabá 68500-000, Brazil

ARTICLE INFO

Article history:

Received 11 October 2016

Received in revised form 20 December 2016

Accepted 28 December 2016

Available online 31 December 2016

Keywords:

Multiaxial fatigue

In-phase proportional loadings

Unified Notch rule

Elastoplastic Finite Element calculations

ABSTRACT

There are several methods or rules to estimate elastoplastic (EP) notch-tip stresses and strains from simpler linear elastic calculations, an almost indispensable step for practical fatigue damage calculations. Neuber's and Molski-Glinka's rules are perhaps the most popular for fatigue analyses of uniaxial load histories. Their use in such elementary cases is relatively easy, but the general case of non-proportional multi-axial load histories require non-trivial incremental plasticity calculations to correlate EP stresses and strains at the notch tip, a quite challenging task. However, for in-phase proportional multi-axial histories, where the principal directions do not change and the load path in a stress diagram follows a straight line, approximate calculation methods can be used to avoid the need for an incremental EP approach. Most of these methods are based on Neuber's rule, so they may result in conservative predictions, in particular under near plane strain-dominated states associated with sharp notches. To minimize this problem, a Unified Notch Rule (UNR) is proposed and evaluated in this work, by comparing its predictions with EP Finite Element calculations on notched shafts, both for uniaxial and for in-phase proportional multi-axial load histories. The UNR can reproduce Neuber's or Molski-Glinka's rules, interpolate their notch-tip behaviors, or even extrapolate them for notches with increased transversal constraint, which affect the plastic behavior at notch tips. Moreover, the UNR can also consider non-zero normal stresses perpendicular to the free-surface.

© 2016 Elsevier Ltd. All rights reserved.

1. Introduction

Most metallic alloys are direction-sensitive materials, which tend to fail due to the growth of a single dominant crack under fatigue loading conditions [1]. The initiation of such cracks under multi-axial loads tends to be better described by critical-plane fatigue-damage models, which search for the material plane at the critical point where a suitable accumulated damage parameter is maximized. These fatigue-damage parameters depend on the stress/strain range and peak histories at those critical points, usually a notch tip, so in practice most fatigue life estimation routines need to correlate nominal load histories with the stress and strain histories they induce at critical notch tips, which in the general case are elastoplastic (EP) [2].

It is relatively simple to estimate EP stress/strain histories at notch tips under *uniaxial* loading conditions for fatigue design

purposes, and even to automate such calculations to deal with variable amplitude loads in a suitable computational code [3]. Neuber's [4–7] and Molski-Glinka's [8] rules are well known and widely used for such purposes. Nevertheless, it is less well known that even in such uniaxial cases they should be used with the due care under high nominal loads [2,9], and/or under high transversal constraints that can induce near plane strain conditions, in special at sharp notch tips. In the latter cases, Stephens et al. recommend the use of the Linear strain concentration rule [10], an idea supported by data measured when developing the Critical Damage model to estimate fatigue crack growth rates from ϵN properties [11,12].

Moreover, the use of Neuber's rule in its classical simplified form $(K_t \Delta \sigma_n)^2 = \Delta \sigma \cdot \Delta \epsilon \cdot E$ to model the effects of high nominal stresses, where $\Delta \sigma_n$ is the nominal stress range that induces EP stress and strain ranges $\Delta \sigma$ and $\Delta \epsilon$ at the notch tip, usually leads to fatigue damage predictions with significant numerical errors. Besides, this is an inconsistent practice even when $\Delta \sigma_n$ can be assumed as purely linear elastic (LE), because this formulation uses two different constitutive equations to describe the same material.

* Corresponding author.

E-mail addresses: meggi@puc-rio.br (M.A. Meggiolaro), jtcastro@puc-rio.br (J.T.P. Castro), lfn@tegraf.puc-rio.br (L.F. Martha), lfernando@unifesspa.edu.br (L.F.N. Marques).

Nomenclature

b	Coffin-Manson's elastic exponent, or width of the cross section of a rectangular beam [mm], or longest branch of a bifurcated crack [μm]	VAL	variable amplitude loading
c	Coffin-Manson's plastic exponent, or 2D crack width (or semi-width) [mm], or shortest branch of a bifurcated crack [μm]	α	Newman's 3D constraint factor (from $\alpha = 1$ in pl- σ to $\alpha = 1/(1 - 2\nu)$ in pl- ε), or thermal expansion coefficient [$\mu\text{m}/(\text{m K})$], or angle [rad]
E	elasticity (or Young's) modulus in tension [GPa], or abbreviation for solved examples	α_{ED}	energy dissipation coefficient
E*	effective Young's modulus ($E^* = E$ under plane stress and $E^* = E/(1 - \nu^2)$ under plane strain) [GPa]	α_U	notch constraint factor
EP	elastoplastic	$\bar{\alpha}_U$	effective notch constraint factor
e_x, e_y, e_z	normal deviatoric strains	$\Delta\varepsilon$	strain range at the critical point
FE, FEM	Finite Elements, Finite Element method	$\Delta\varepsilon_n$	nominal strain range
FE_s	element size [mm]	$\Delta\sigma$	stress range at the critical point [MPa]
h_c, H_c	cyclic strain-hardening exponent and coefficient [1, MPa]	$\Delta\sigma_n$	nominal stress range [MPa]
H_c^*	effective cyclic strain-hardening coefficient [MPa]	$\varepsilon_1, \varepsilon_2, \varepsilon_3$	principal strains
K_t	linear elastic (or geometric) stress concentration factor	$\bar{\varepsilon}$	pseudo-strain (Hookean value calculated using the theory of elasticity)
$K_{t\sigma}$	stress concentration factor for tension	ε_c	Coffin-Manson's plastic coefficient
$K_{t\tau}$	stress concentration factor for torsion	$\varepsilon_x, \varepsilon_y, \varepsilon_z$	normal strains
K_ε	elastoplastic strain concentration factor	ϕ_2, ϕ_3	biaxiality ratios $\varepsilon_2/\varepsilon_1$ and $\varepsilon_3/\varepsilon_1$ between principal strains
K_σ	elastoplastic stress concentration factor	λ_2, λ_3	biaxiality ratios σ_2/σ_1 and σ_3/σ_1 between principal stresses
LE	linear elastic	ν	Poisson ratio (or Poisson coefficient)
LIFO	last-in-first-out	$\bar{\nu}$	effective Poisson ratio
N	life (in number of cycles)	ρ	notch tip radius [mm]
P_i	generalized plastic modulus of each hardening surface i from Mróz [MPa]	$\bar{\sigma}$	pseudo-stress (Hookean value calculated using the theory of elasticity) [MPa]
r_i	radius of each hardening surface i [MPa]	$\sigma_1, \sigma_2, \sigma_3$	principal stresses [MPa]
RMSe	root mean square error [%]	σ_c	Coffin-Manson's elastic coefficient [MPa]
$R_{\tau\sigma}$	proportionality stress ratio	σ_n	nominal stress [MPa]
S_x, S_y, S_z	normal deviatoric stresses [MPa]	$\sigma_x, \sigma_y, \sigma_z$	normal stresses [MPa]
S_{yc}	cyclic yield strength [MPa]	τ	shear stress [MPa]
UNR	unified notch rule	$\tau_{xy}, \tau_{xz}, \tau_{yz}$	shear stresses [MPa]
		θ	cylinder sector cutting angle [deg]
		\sim	pseudo-values

Indeed, the usual practice of correlating $\Delta\sigma_n$ with $\Delta\varepsilon_n$ by Hooke's law and using Ramberg-Osgood (which does not recognize purely LE strains) to model the $\Delta\sigma\Delta\varepsilon$ loops they induce at the notch tip, is at least inelegant even when $\Delta\sigma_n \ll 2S_{yc}$, where S_{yc} is the cyclic yield strength of the material. Moreover, under higher loads when the nominal stress $\Delta\sigma_n$ is EP, Neuber's rule clearly cannot be used in that simplified form. These problems must be modeled by a system of three equations containing Neuber and two Ramberg-Osgood equations, one to describe the $\Delta\sigma\Delta\varepsilon$ loops at the notch tip, and the other to model the nominal $\Delta\sigma_n\Delta\varepsilon_n$ loops:

$$\begin{cases} K_t^2 = \Delta\sigma\Delta\varepsilon/\Delta\sigma_n\Delta\varepsilon_n \\ \Delta\varepsilon = (\Delta\sigma/E) + 2(\Delta\sigma/2H_c)^{1/h_c} \\ \Delta\varepsilon_n = (\Delta\sigma_n/E) + 2(\Delta\sigma_n/2H_c)^{1/h_c} \end{cases} \quad (1)$$

Contrary to what might be anticipated, this 3-equation system does not overburden fatigue life calculations, which remain almost identical to those used with the simplified LE $\Delta\sigma_n$ hypothesis: fatigue damage can be estimated by first obtaining the notch-tip stress range $\Delta\sigma$ from the nominal EP ranges $\Delta\sigma_n$ and $\Delta\varepsilon_n$, using Neuber and Ramberg-Osgood; then the corresponding $\Delta\varepsilon$ range from Ramberg-Osgood again; and finally the life N from Coffin-Manson or another suitable εN rule:

$$\begin{aligned} K_t^2 \left[\Delta\sigma_n^2 + 2E\Delta\sigma_n \left(\frac{\Delta\sigma_n}{2H_c} \right)^{1/h_c} \right] &= \Delta\sigma^2 + 2E\Delta\sigma \left(\frac{\Delta\sigma}{2H_c} \right)^{1/h_c} \Rightarrow \\ \Rightarrow \Delta\varepsilon &= \frac{\Delta\sigma}{E} + 2 \cdot \left[\frac{\Delta\sigma}{2H_c} \right]^{1/h_c} = \frac{2\sigma_c}{E} (2N)^b + 2\varepsilon_c (2N)^c \end{aligned} \quad (2)$$

The minimum value the stress concentration factor K_σ can reach under high loads according to this consistent EP formulation for Neuber's system occurs when the elastic ranges are negligible:

$$K_t^2 \left[\frac{2E\Delta\sigma_n^{(h_c+1)/h_c}}{(2H_c)^{1/h_c}} \right] = \frac{2E\Delta\sigma^{(h_c+1)/h_c}}{(2H_c)^{1/h_c}} \Rightarrow K_{\sigma,\min} = \frac{\Delta\sigma}{\Delta\sigma_n} = K_t^{2h_c/(1+h_c)} \quad (3)$$

Since by Neuber's rule $K_t^2 = K_\sigma K_\varepsilon$, the corresponding maximum EP strain concentration factor calculated considering a Ramberg-Osgood material is $K_{\varepsilon,\max} = K_t^2/K_t^{2h_c/(1+h_c)} = K_t^{2/(1+h_c)}$, see Fig. 1. Hence, the uniaxial K_σ and K_ε predicted by this consistent Neuber's rule formulation should be limited by the bounds:

$$\begin{cases} K_t^{2h_c/(1+h_c)} \leq K_\sigma \leq K_t \\ K_t \leq K_\varepsilon \leq K_t^{2/(1+h_c)} \end{cases} \quad (K_\sigma \text{ and } K_\varepsilon \text{ defined with respect to EP nominal stresses}) \quad (4)$$

Fig. 2 shows the *non-conservative* error curves $err_{\Delta\sigma} = (\Delta\sigma_{LE} - \Delta\sigma_{EP})/\Delta\sigma_{EP}$ resulting from the use of LE nominal stress ranges in Neuber's system to predict the corresponding maximum stress ranges at a notch tip with $K_t = 3$. These error curves are presented as a function of the $\Delta\sigma_n/2S_{yc}$ ratio, for each one of 517 steels whose properties are described in [13].

Fig. 3 presents still more relevant errors (which, once again, are always *non-conservative*) induced by modeling $\Delta\sigma_n$ as LE when estimating the resulting fatigue crack initiation lives N by Coffin-Manson procedures, defining these errors by $err_N = (N_{LE} - N_{EP})/N_{EP}$. All these curves were calculated using measured cyclic properties of 517 steels as discussed in [13], so they reflect the influence

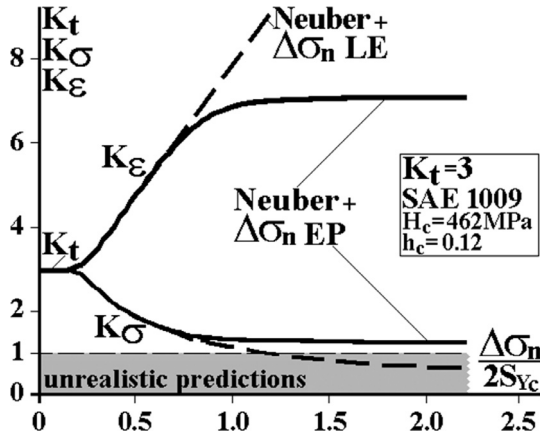


Fig. 1. Unlike the usual LE $\Delta\sigma_n$ formulation, which may lead to unrealistic predictions like $K_\sigma < 1$, the EP $\Delta\sigma_n$ formulation from Eq. (1) predicts that both the stress and the strain concentration factors K_σ and K_ε tend to limit values given by Eq. (4) at very high $\Delta\sigma_n/2S_{yc}$ ratios.

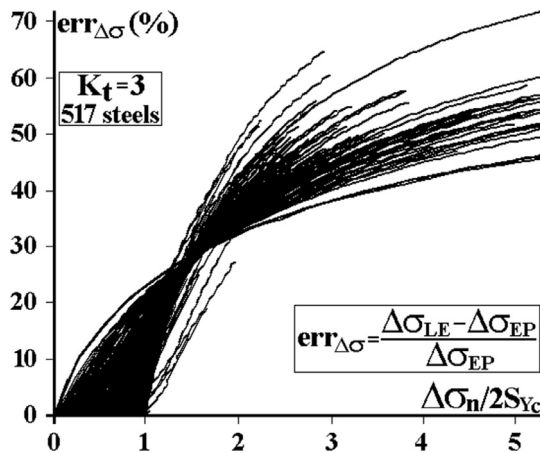


Fig. 2. The non-conservative errors $err_{\Delta\sigma} = (\Delta\sigma_{LE} - \Delta\sigma_{EP})/\Delta\sigma_{EP}$ in ranges $\Delta\sigma$ predicted at notch tips by modeling $\Delta\sigma_n$ as LE can be large even when $\Delta\sigma_n/2S_{yc} < 1$.

of the Neuber formulation on the predicted stress range and the consequent fatigue life initiation, for $K_t = 3$. Notice that even for low nominal ranges $\Delta\sigma_n \ll 2S_{yc}$, this life estimation error can be very large in many steels, a certainly most undesirable situation, which can lead to unsafe non-conservative decisions.

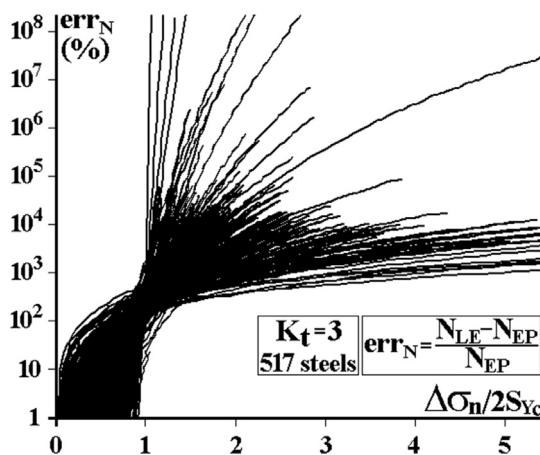


Fig. 3. The non-conservative errors $err_N = (N_{LE} - N_{EP})/N_{EP}$ in predicted crack initiation lives modeling $\Delta\sigma_n$ as LE can be very large: in average 213% for $\Delta\sigma_n/2S_{yc} = 1$.

Note that the curves in Figs. 2 and 3 are plotted only until the notch stress amplitude reaches the true rupture stress of each material. In some very ductile materials, the ratio $\Delta\sigma_n/2S_{yc}$ can reach values higher than 5, for two reasons: (i) such $\Delta\sigma_n/2$ amplitudes are modeled as true stresses, associated with true rupture stresses that can be much higher than the ultimate strength S_U and cyclic yield strength S_{yc} (which are based on engineering stresses), especially for very ductile materials; and (ii) the elastoplastic stress concentration factor can be much smaller than the linear-elastic value $K_t = 3$ used in these figures, tending to 1.0 under very high $\Delta\sigma_n/2S_{yc}$ stress ratios.

It is not uncommon to find notched components that suffer elastoplastic nominal stress cycles, especially when made of the tough steels used in the automotive industry. Many high toughness and high ductility steels can endure millions of cycles even under elastoplastic notch stresses. If, on top of that, the studied component has very mild notches, which is often the case in well-designed or optimized profiles, then such long fatigue lives used in practical applications can also be associated with elastoplastic nominal stresses, which requires them to be modeled using e.g. Ramberg-Osgood instead of Hooke's law. Moreover, under variable amplitude loadings it is not completely uncommon to have gross yielding of the nominal section due to unexpected sparse overloads, which could still be associated with long fatigue lives if they are rare events. In these overload events, proper calculations using Ramberg-Osgood for both nominal and notch-root stresses are needed to avoid numerical errors, which can be, as shown above, very significant.

Likewise, Molski-Glinka's rule can be applied to describe EP stress/strain concentration effects by modeling the hysteresis loops $\Delta\sigma\Delta\varepsilon$ induced by the loading at the critical notch tip assuming LE nominal stresses using Eq. (5):

$$(K_t \Delta\sigma_n)^2 = \Delta\sigma^2 + \frac{4E}{(1+h_c)(2H_c)^{1/h_c}} \Delta\sigma^{(h_c+1)/h_c} \quad (5)$$

Since $4E/(1+h_c) < 2E$, the EP stresses and strains estimated by Molski-Glinka at notch tips are always smaller than those estimated by Neuber, and larger than those estimated by the Linear strain concentration rule, which assumes $K_\varepsilon = K_t$. However, as pointed out above for Neuber's rule, the LE $\Delta\sigma_n$ hypothesis is only appropriate to model low nominal stress ranges, much lower than the cyclic yield strength range ΔS_{yc} . Otherwise, stress/strain concentration rules should model both nominal and notch-tip stress-strain relations as EP, using e.g. Ramberg-Osgood's equation. Under such conditions, Molski-Glinka's rule applied to the $\Delta\sigma\Delta\varepsilon$ loop curve becomes

$$K_t^2 \cdot \left(\Delta\sigma_n^2 + \frac{4E\Delta\sigma_n}{1+h_c} \left(\frac{\Delta\sigma_n}{2H_c} \right)^{1/h_c} \right) = \Delta\sigma^2 + \frac{4E\Delta\sigma}{1+h_c} \left(\frac{\Delta\sigma}{2H_c} \right)^{1/h_c} \quad (6)$$

Before proceeding, let's emphasize two points about all these simplified procedures: first, EP stress/strain concentration rules are just educated estimates for EP notch effects based on unique LE K_t values. These rules provide reasonable but certainly not very precise estimates for K_σ and K_ε . Better estimates only can be obtained by numerically calculating EP $\Delta\sigma$ and $\Delta\varepsilon$ ranges using (e.g.) advanced 3D FE techniques, which require erudition and must be used with caution. In fact, such calculations are neither trivial nor robust, as discussed later on. As K_σ and K_ε depend not only on the geometry, but also on how and how much the material strain-hardens, it is certainly better to whenever possible calibrate them experimentally. Moreover, for very large strains the notch tip radius can vary and affect K_σ and K_ε values along the loading/unloading path. Such points are further discussed in [2,9].

However, to apply such simplified EP stress/strain concentration rules under uniaxial but variable amplitude loading conditions

(VAL) is not that easy. Efficient uniaxial εN -based VAL fatigue damage calculations for un-notched components were initially proposed on the pioneer work by Martin, Topper, and Sinclair [14]. The routines implemented in [3], which also use several elements from the 4-point rainflow algorithm [15,16], are illustrated in Fig. 4. This algorithm is called “real time rainflow” because it is able to calculate the hysteresis loops, rainflow-count them, and obtain the resulting fatigue damage in real time, as the stresses or strains are input into the computer, without the need to know the entire load history beforehand. Indeed, if implemented in a portable computer connected to a strain measurement system, this algorithm would be able to display in real time the damage so far induced in the instrumented point, a really amazing potential feature.

In the εN real-time rainflow algorithm, for a given uniaxial stress history composed by a series of discrete events $\{\sigma_i, i = 0, 1, 2, \dots, n$,

each element σ_i (e.g. the peaks and valleys of the load history) is sequentially inserted at the bottom of a memory stack, leaving the ε_i value blank. The maximum absolute value of the stress σ_i so far (from the event zero until the current event i) is then stored at $|\sigma|_{\max}$, whose initial value is null. After the insertion of each stress σ_i , all stack rows that need to be eliminated according to the rules from Fig. 4 must be removed from the list, while the events counted in this process are stored and their associated damage is computed. The state shown on the upper right of Fig. 4 (top) happens every time the critical point stresses (or strains) stored in the stack variable s_k are such that $s_{k-1} < s_{k-2} \leq s_k$, with a number of lines $k > 3$ in the stack. As shown in the figure, one load cycle can be counted between the states s_{k-1} and s_{k-2} , which are then eliminated from their stack position between states s_{k-3} and s_k . The other condition $s_{k-1} > s_{k-2} \geq s_k$ with $k > 3$ is simply the symmetric case, when the

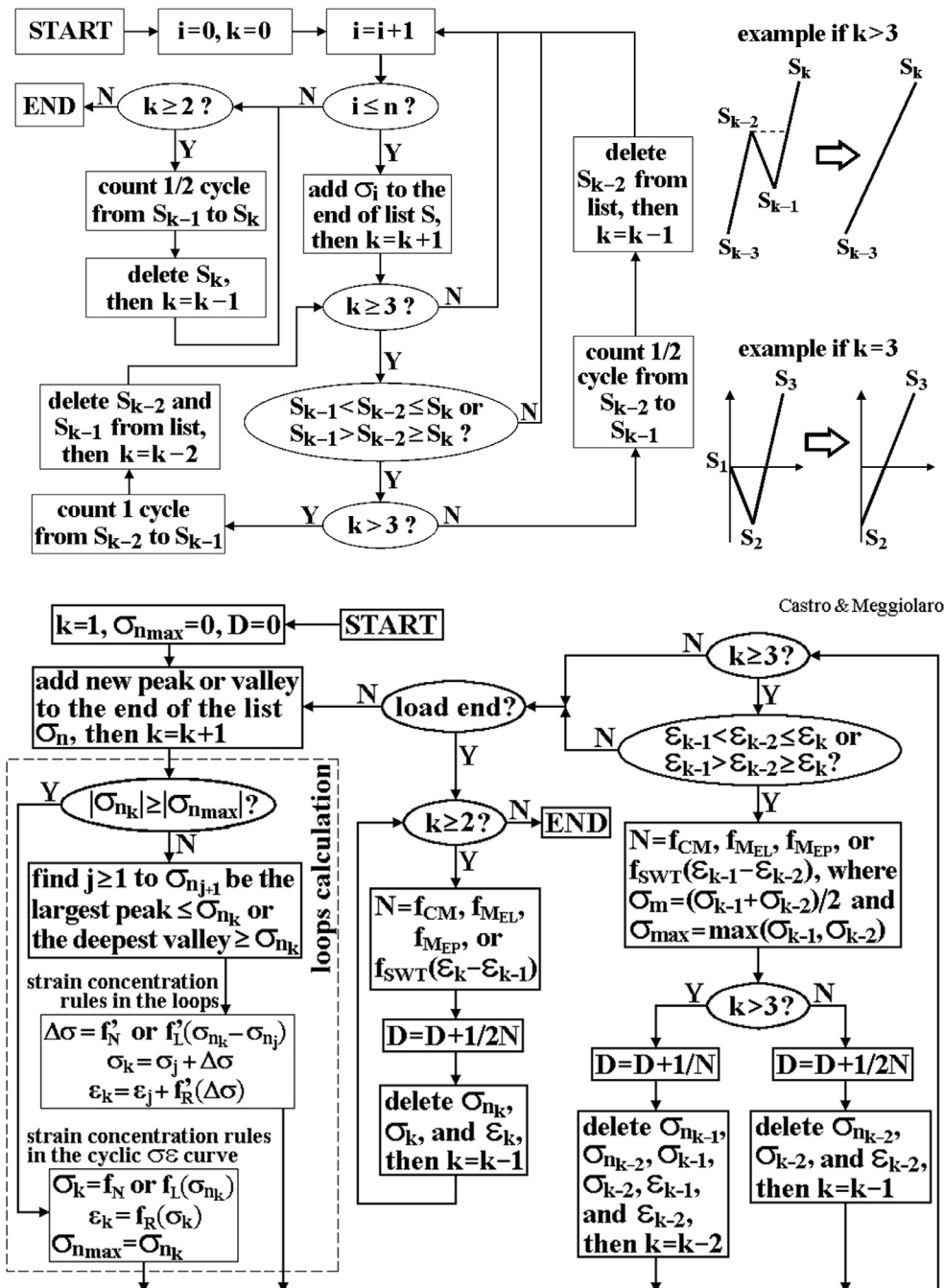


Fig. 4. Real-time rainflow algorithm flowcharts, applied to the SN (top) and εN (bottom) methods.

load is decreasing ($s_{k-3} > s_k$) instead of increasing. All cycles counted in this way are the ones that a traditional rainflow algorithm would have identified, namely stop an ongoing count when a previously started counting sequence is found. Further details, including numerical examples, can be found in [2].

The algorithm goes on until the end of the VAL stress history. Then, the remaining stack rows that were not eliminated from these two criteria have to be rainflow-counted. As shown in Fig. 4, a half-cycle is counted for every remaining consecutive pair of states s_{k-1} and s_k , as long as there are still $k \geq 2$ lines remaining in the stack. Such counted half-cycles are equivalent to the last criterion from the traditional rainflow algorithm, namely a count should be stopped when reaching the end of the load history. In the end, all cycles and half-cycles will have been identified, without repetition and without missing any of them.

This real time rainflow algorithm is so powerful that it is able to calculate all the EP hysteresis loops under uniaxial VAL considering the switching from cyclic to loop curves and vice versa, closing the (as assumed by classic εN procedures) symmetric Masing loops and returning the strain amplitudes from rainflow-counted half-cycles automatically. Notice that unlike the sequential rainflow method [2], this algorithm is not sequentially ordered by the last counting point. However, to reproduce the same output of a sequential rainflow algorithm, it is enough to reorder from 1 to n the output half-cycles by their final counting point. Curiously, such a Last-In-First-Out (LIFO) listing adopted for the memory stack exactly reproduces but predates the rainflow method – it has long been applied to railway yard shunting and many other queuing problems.

For a given strain history $\{\varepsilon_i\}$ instead of stress, the strain-based real-time rainflow algorithm is almost identical, except that the corresponding stress components σ_i are calculated from each strain event ε_i , instead of the opposite, with the choice between using the cyclic $\sigma\varepsilon$ or the loop $\Delta\sigma\Delta\varepsilon$ curves depending on the values of the current $|\varepsilon_i|$ and of the maximum absolute strain $|\varepsilon|_{\max}$ stored so far, instead of on the $|\sigma_i|$ and $|\sigma|_{\max}$ values, as in the stress-based algorithm. The algorithm essentially remains the same, except that its memory stack will store in each row, instead of the pairs $\{\sigma_i, \varepsilon_i\}$, the triplets $\{\sigma_{ni}, \sigma_i, \varepsilon_i\}$ for a given nominal stress history $\{\sigma_{ni}\}$, or $\{\varepsilon_{ni}, \sigma_i, \varepsilon_i\}$ for a given nominal strain history $\{\varepsilon_{ni}\}$. The notch-tip strain ε_i continues to be the variable stored in each stack variable s_k from Fig. 4.

For a given nominal stress history $\{\sigma_{ni}\}$, $i = 0, 1, 2, \dots, n$, each nominal stress event σ_{ni} is sequentially inserted at the bottom of the memory stack, leaving blank the unknown notch-tip stress σ_i and strain ε_i . The maximum absolute value of the nominal stress σ_{ni} so far is stored at the $|\sigma_n|_{\max}$ stack, whose initial value is zero. After the insertion of each nominal stress σ_{ni} , all stack rows that need to be eliminated according to the εN -based algorithm described in Fig. 4 (bottom) must be removed from the list, while the eventually counted cycles or half-cycles in this process are stored and their associated damage computed. After (and only after) the removal of these stack rows, the missing notch-tip stresses and strains σ_i and ε_i from the bottom row of the stack can be calculated:

- if the current $|\sigma_{ni}| \geq |\sigma_n|_{\max}$, then σ_i and ε_i must be calculated using the cyclic $\sigma\varepsilon$ curve, the current nominal σ_{ni} , and the chosen EP stress/strain concentration rule (Neuber, Molski-Glinka, Linear, or any other), while $|\sigma_n|_{\max}$ is updated to the new maximum nominal value $|\sigma_{ni}|$; or else
- if the current $|\sigma_{ni}| < |\sigma_n|_{\max}$, then the EP loop follows the loop $\Delta\sigma\Delta\varepsilon$ curve that departed from the point from the stack row right above it, whose nominal range $\Delta\sigma_n$ is described by the difference between their nominal stresses, solving for the notch $\Delta\sigma_i$ and $\Delta\varepsilon_i$ using the chosen concentration rule.

If a VAL nominal strain history $\{\varepsilon_{ni}\}$ instead of nominal stress is given, the algorithm is almost identical, except that the notch-tip stresses and strains σ_i and ε_i are calculated from each ε_{ni} (instead of σ_{ni}), depending on the values of the current $|\varepsilon_{ni}|$ and the maximum absolute nominal strain $|\varepsilon_n|_{\max}$ so far, instead of $|\sigma_{ni}|$ and $|\sigma_n|_{\max}$. Notice that both the peak and the range values of each load event are properly quantified in this process, a necessary feature to account for mean or peak effects in fatigue damage calculations.

In principle, the conditions $s_{k-1} < s_{k-2} \leq s_k$ and $s_{k-1} > s_{k-2} \geq s_k$ from Fig. 4 should always be evaluated from the stack variables s_k containing the notch-tip strains ε_i . However, the ε_i from the bottom row of the stack may still be unknown, since it can only be calculated after the removal of all closed loops and their associated stack rows. Indeed, notch-tip strains monotonically increase (or decrease) under uniaxial loading altogether with not only their notch-tip stresses, but also with their associated nominal stresses and strains. All simply connected structures made of Masing materials have load-deformation behaviors related by a Masing model [17]. Therefore, the topology of the Masing nominal stress vs. nominal strain EP loops and of the notch stress vs. notch strain loops are equal, including all its curve changes, loops that close, and their relative order along the history. This equivalence of Masing loops is valid even for mixed plots such as nominal stress vs. notch-tip strain, or force vs. deflection, as long as they are caused by the same uniaxial load history. So, the inequalities $s_{k-1} < s_{k-2} \leq s_k$ and $s_{k-1} > s_{k-2} \geq s_k$ from the algorithm can also be evaluated with the given nominal σ_{ni} or ε_{ni} (instead of the notch-tip strain ε_i) histories without altering the results. In this way, these inequalities can be evaluated even before the notch strains ε_i induced by them are calculated. Once again, Ref. [2] can be consulted for further details and numerical examples.

2. Multiaxial loading issues

The problem of calculating EP stresses and strains at notch tips induced by a given nominal multiaxial stress or strain history is in general much more complicated than the uniaxial problem, even when modeling well behaved Masing materials. To deal with such problems it is usually necessary to adopt an incremental plasticity formulation, thus a calculation scheme that sequentially integrates non-linear differential equations to obtain the required stress-strain behavior [18–21]. In general this is a far from an elementary task, in particular when dealing with local EP concentration effects at notch tips. However, a much simpler approach can be used in some simpler cases to generalize the idea behind the uniaxial concentration rules: to perform a single global linear elastic (LE) Finite Element (FE) calculation on the entire piece for a static unit value of each applied loading. The resulting values at the notch roots can be called pseudo-stresses and pseudo-strains, fictitious quantities calculated using the theory of elasticity at the critical point of the piece assuming the material follows Hooke's law [22,23]. These pseudo-values, which are represented here with a “~” symbol on top of each variable, consider the multiaxial LE stress/strain concentration effects induced by the notch, but not the local yielding effects induced by higher loads.

In the case of in-phase proportional multiaxial loadings, a particular but nevertheless important problem in many practical applications, approximate models to estimate suitable EP stress and strain concentration factors K_σ and K_ε can then be used to avoid the need for computationally-intensive incremental plasticity calculations. They provide notch-tip corrections that try to correlate pseudo and EP stresses and strains using a scalar parameter such as the von Mises equivalent stress. The main EP models to estimate notch-tip concentration effects induced by in-phase

proportional histories are the constant ratio [1], Hoffmann-Seeger's [24,25], and Dowling's [26] models, defined using the following notation:

- $\bar{\sigma}_i$ and $\bar{\varepsilon}_i$: pseudo principal stresses and strains at the notch tip, where $i = 1, 2, 3$.
- σ_i and ε_i : actual EP principal stresses and strains at the notch tip.
- λ_2 and λ_3 : biaxiality ratios between principal stresses, $\lambda_2 \equiv \sigma_2/\sigma_1$ and $\lambda_3 \equiv \sigma_3/\sigma_1$, both assumed between -1 and 1 .
- ϕ_2 and ϕ_3 : biaxiality ratios between principal strains, where $\phi_2 \equiv \varepsilon_2/\varepsilon_1$ and $\phi_3 \equiv \varepsilon_3/\varepsilon_1$, also assumed between -1 and 1 ; and
- $\bar{\nu}$: effective Poisson ratio, with $\nu < \bar{\nu} \leq 0.5$ in the EP case.

It must be pointed out that the traditional Hoffmann-Seeger's model is also widely used in practice. Moreover, some other recent notch stress-strain models have been proposed by Salemi and Kujawski [27], by Ince [28], and by Marangon, Campagnolo and Berto [29]. However, this paper will detail only Dowling's model, since the proposed UNR can be seen as a generalization of its procedures. Dowling's model assumes that the principal stresses σ_1 and σ_2 act on the free surface of the critical point (where $\sigma_3 = 0$), but it considers that both λ_2 and ϕ_2 remain constant, thus can be estimated from the pseudo-stresses and pseudo-strains:

$$\lambda_2 = \frac{\sigma_2}{\sigma_1} \cong \frac{\bar{\sigma}_2}{\bar{\sigma}_1} \cong \frac{\phi_2 + \nu}{1 + \phi_2 \nu}, \quad \phi_2 = \frac{\varepsilon_2}{\varepsilon_1} \cong \frac{\bar{\varepsilon}_2}{\bar{\varepsilon}_1} \cong \frac{\lambda_2 - \nu}{1 - \lambda_2 \nu} \quad (7)$$

So, Dowling's model can then directly correlate σ_1 and ε_1 , using effective Ramberg-Osgood parameters E^* and H_c^* to describe the strain-hardening behavior of the material:

$$\varepsilon_1 = \frac{\sigma_1}{E^*} + \left[\frac{\sigma_1}{H_c^*} \right]^{1/h_c} \quad (8)$$

$$E^* = E \cdot \left(\frac{1 + \phi_2 \nu}{1 - \nu^2} \right), \quad H_c^* = H_c \cdot \frac{(1 - \lambda_2 + \lambda_2^2)^{(h_c-1)/2}}{(1 - \lambda_2/2)^{h_c}} \quad (9)$$

In notched components, assuming that the principal directions of the EP stresses and pseudo-stresses are equal, a variation of Neuber's rule [4] can then be used to estimate the EP notch-tip principal stress σ_1 (and then the consequent strain ε_1) from the pseudo-stress $\bar{\sigma}_1$:

$$\bar{\sigma}_1 \cdot \left[\frac{\bar{\sigma}_1}{E} \right] = \bar{\sigma}_1 \cdot \bar{\varepsilon}_1 = \sigma_1 \cdot \varepsilon_1 = \sigma_1 \cdot \left[\frac{\sigma_1}{E^*} + \left(\frac{\sigma_1}{H_c^*} \right)^{1/h_c} \right] \quad (\text{Dowling}) \quad (10)$$

The above equation does not require a plastic term on the left hand side, because the pseudo-stresses and pseudo-strains are, by definition, LE. Finally, the other notch-tip EP principal stresses and strains are then obtained from σ_1 and ε_1 :

$$\begin{cases} \sigma_2 = \lambda_2 \sigma_1, & \sigma_3 = 0 \\ \varepsilon_2 = \phi_2 \varepsilon_1, & \varepsilon_3 = -\bar{\nu} \varepsilon_1 \frac{1+\lambda_2}{1-\lambda_2 \bar{\nu}}, \quad \bar{\nu} = 0.5 - (0.5 - \nu) \frac{\sigma_1}{E^* \varepsilon_1} \end{cases} \quad (11)$$

3. The Uniaxial Unified Notch Rule (UNR)

Noting that often Molski-Glinka's rule [8] tends to underestimate while Neuber's rule [4] tends to overestimate notch-tip EP stresses and strains, when compared to experimental results and to FE analyses, Ye, Hertel, and Vormwald proposed a unified stress/strain incremental concentration rule that returns values in-between them [30]. For a monotonic uniaxial loading in the x direction, their rule states that

$$\sigma_x d\bar{\varepsilon}_x \cdot (1 + \alpha_{ED}) + \varepsilon_x d\sigma_x \cdot (1 - \alpha_{ED}) = \bar{\sigma}_x d\bar{\varepsilon}_x + \bar{\varepsilon}_x d\bar{\sigma}_x \quad (12)$$

where $0 \leq \alpha_{ED} \leq 1$ was called the energy dissipation coefficient, assumed in [30] as a material parameter, estimated from $\alpha_{ED} \cong (1 - 2h_c)/(1 - h_c)$ based on an energy argument, where h_c is the cyclic strain-hardening exponent of Ramberg-Osgood's equation.

However, α_{ED} might depend not only on the material but also on the notch geometry and on its plasticity constraint factor, a parameter that quantifies thickness-induced restrictions on the plastic flow around its tip. This coefficient α_{ED} can also be regarded as a fitting parameter, if experimental data or reliable EP FE analyses are available for its calibration. Based on these ideas, a deviatoric version of Eq. (12) is proposed in this work:

$$s_x d\varepsilon_x \cdot (\alpha_U) + e_x d\varepsilon_x \cdot (2 - \alpha_U) = \bar{s}_x d\bar{\varepsilon}_x + \bar{e}_x d\bar{\varepsilon}_x \quad (13)$$

where $s_x \equiv (2\sigma_x - \sigma_y - \sigma_z)/3$ and $e_x \equiv (2\varepsilon_x - \varepsilon_y - \varepsilon_z)/3$ are deviatoric stresses and strains in the x direction, while $\alpha_U \equiv (1 + \alpha_{ED})$ is called the notch constraint factor, with values $1 \leq \alpha_U \leq 2$ to interpolate between the Incremental Neuber rule [31–33] (for which $\alpha_U = 1$) and the similarly defined Incremental Molski-Glinka rule (for which $\alpha_U = 2$).

As the deviatoric stresses s_x , s_y and s_z are linearly dependent, since $s_x + s_y + s_z = 0$, it is possible to reduce the deviatoric stress and strain space dimensions using:

$$s_1 \equiv \sigma_x - \frac{\sigma_y + \sigma_z}{2} = \frac{3}{2} s_x, \quad s_2 \equiv \frac{\sigma_y - \sigma_z}{2} \sqrt{3} = \frac{s_y - s_z}{2} \sqrt{3} \quad (14)$$

$$e_1 \equiv \varepsilon_x - \frac{\varepsilon_y + \varepsilon_z}{2} = \frac{3}{2} e_x, \quad e_2 \equiv \frac{\varepsilon_y - \varepsilon_z}{2} \sqrt{3} = \frac{e_y - e_z}{2} \sqrt{3} \quad (15)$$

Assuming that Eq. (13) can be applied to the deviatoric stresses and strains described in Eqs. (14) and (15), then it is possible to write that

$$\begin{cases} (\alpha_U) \cdot s_1 d\varepsilon_1 + (2 - \alpha_U) \cdot e_1 d\varepsilon_1 = \bar{s}_1 d\bar{\varepsilon}_1 + \bar{e}_1 d\bar{\varepsilon}_1 \\ (\alpha_U) \cdot s_2 d\varepsilon_2 + (2 - \alpha_U) \cdot e_2 d\varepsilon_2 = \bar{s}_2 d\bar{\varepsilon}_2 + \bar{e}_2 d\bar{\varepsilon}_2 \end{cases} \quad (16)$$

where, as explained before, the symbol “ \sim ” is used for the pseudo stress/strain values calculated from LE analyses, which consider multiaxial LE stress/strain concentration effects induced by the notch, but not the local yielding effects induced by higher loads.

Finally, the Unified Notch Rule (UNR) proposed in this work can then be obtained from the integration of Eq. (16), which can be used for both uniaxial and in-phase proportional histories. For uniaxial histories, this integration results in the scalar UNR:

$$\bar{\varepsilon}^2 = \frac{\sigma}{E} \cdot \left[\frac{\sigma}{E} + \bar{\alpha}_U \cdot \left(\frac{\sigma}{H_c} \right)^{1/h_c} \right], \quad \bar{\alpha}_U \equiv \frac{\alpha_U + h_c(2 - \alpha_U)}{1 + h_c} \quad (\text{UNR}) \quad (17)$$

where $\bar{\alpha}_U$ is the effective notch constraint factor.

Eq. (17) can reproduce Neuber for $\alpha_U = 1$ (and thus $\bar{\alpha}_U = 1$), and Glinka's rule for $\alpha_U = 2$ (and thus $\bar{\alpha}_U = 2/(1 + h_c)$). Moreover, it is interesting to note that, although conceptually different, the parameter α_U shares some similarities with Newman's constraint factor α in his ΔK_{eff} -based strip-yield model for FCG [34], which vary from 1.0 under plane stress (where Neuber's rule is recommended) up to 3.0 or even more under plane strain conditions at the notch tip: both α_U and Newman's α reflect the effect of increased transversal constraint induced by the stress state and somehow account for the associated plasticity decrease at the critical point, although clearly α_U must be used for notch and Newman's α for crack tips.

4. The multiaxial unified notch rule

The multiaxial version of the UNR proposed here assumes in-phase proportional loading under free-surface conditions and $\tau_{xz} = \tau_{yz} = 0$, but allows the presence of a surface normal $\sigma_z \neq 0$, where the z axis is assumed perpendicular to the surface, and the

x and y axes are aligned with the remaining principal directions, with x in the direction of the maximum absolute principal stress. Therefore, the principal stresses $\sigma_x \equiv \sigma_1$, $\sigma_y \equiv \sigma_2$, and $\sigma_z \equiv \sigma_3$ are assumed to satisfy $|\sigma_x| \geq |\sigma_y|$ and $|\sigma_x| \geq |\sigma_z|$ during the entire load history. The involved variables are the same as the ones defined before, in addition to an elastic and plastic separation of the strain biaxiality ratios, through:

- $\phi_{2el} \equiv \varepsilon_{2el}/\varepsilon_{1el}$ and $\phi_{3el} \equiv \varepsilon_{3el}/\varepsilon_{1el}$: biaxiality ratios between principal elastic strains, both assumed between -1 and 1 ; and
- $\phi_{2pl} \equiv \varepsilon_{2pl}/\varepsilon_{1pl}$ and $\phi_{3pl} \equiv \varepsilon_{3pl}/\varepsilon_{1pl}$: same definition, biaxiality ratios between principal elastic strains (note that for pressure-insensitive materials, where $\varepsilon_{1pl} + \varepsilon_{2pl} + \varepsilon_{3pl} = 0$, such as in most metallic alloys, it follows that $1 + \phi_{2pl} + \phi_{3pl} = 0$ and thus $\phi_{2pl} + \phi_{3pl} = -1$).

Since the multiaxial loading history is assumed here to be proportional, the deviatoric stress increment is always parallel to the plastic straining direction, so the Prandtl-Reuss plastic flow rule [1,2] gives, for the normal deviatoric strain components,

$$\begin{bmatrix} de_1 \\ de_2 \end{bmatrix} = \begin{bmatrix} d\varepsilon_{xpl} - (d\varepsilon_{ypl} + d\varepsilon_{zpl})/2 \\ (d\varepsilon_{ypl} - d\varepsilon_{zpl}) \cdot \sqrt{3}/2 \end{bmatrix} = \frac{1}{P} \cdot \begin{bmatrix} d\sigma_x - (d\sigma_y + d\sigma_z)/2 \\ (d\sigma_y - d\sigma_z) \cdot \sqrt{3}/2 \end{bmatrix} \quad (18)$$

where P is called the generalized plastic modulus (proportional to the slope of the stress vs. plastic strain curve at the current stress state), and all shear increments are zero since x , y , and z are defined in the principal directions. Integrating this equation using the plastic biaxiality ratio definitions, then

$$\int_0^{\varepsilon_{xpl}} d\varepsilon_{xpl} \cdot \begin{bmatrix} 1 - (\phi_{2pl} + \phi_{3pl})/2 \\ (\phi_{2pl} - \phi_{3pl}) \cdot \sqrt{3}/2 \end{bmatrix} = \int_0^{\sigma_x} \frac{1}{P} \cdot d\sigma_x \cdot \begin{bmatrix} 1 - (\lambda_2 + \lambda_3)/2 \\ (\lambda_2 - \lambda_3) \cdot \sqrt{3}/2 \end{bmatrix} \quad (19)$$

Hencky-Ilyushin's total strain history could have been used instead to obtain the plastic strains from the stress history, since it is applicable to in-phase proportional loading histories (but not to non-proportional loadings). Nevertheless, Prandtl-Reuss' flow theory was adopted above to better describe the material kinematic hardening under cyclic loads, using e.g. a multi-surface model. Hence, neglecting isotropic hardening transients, assuming that the material follows Ramberg-Osgood with cyclic coefficient and exponent H_c and h_c , and that this proportional loading is balanced, i.e. it does not cause ratcheting or mean stress relaxation, then a Mróz multi-surface hardening model can be adopted instead of the more general non-linear kinematic hardening models [1,2]. To improve the calculation accuracy, let's adopt an infinite number of hardening surfaces, as discussed by Chu in [35], see Fig. 5. From the calibration of the Mróz model, the generalized plastic modulus $P = P_i$ for the hardening surface with radius r_i becomes

$$P_i = (2/3) \cdot h_c H_c (r_i/H_c)^{1-1/h_c} \quad (20)$$

Consider a monotonic proportional loading departing from the origin of the deviatoric stress space, as shown in Fig. 5, assuming x , y and z as principal directions. In this case, the radius r_i of the current active surface from the Mróz model is equal to the norm (and thus the von Mises equivalent value) of the current stress state. Replacing the values of $P = P_i$ and r_i into Eq. (20), and using the plastic strain incompressibility condition $\phi_{2pl} + \phi_{3pl} = -1$, it follows that

$$\bar{\sigma}_1 \cdot \left[\frac{\bar{\sigma}_1}{E^*} \right] = \sigma_1 \cdot \left[\frac{\sigma_1}{E^*} + \bar{\alpha}_U \cdot \left(\frac{\sigma_1}{H_c^*} \right)^{1/h_c} \right] \quad (21)$$

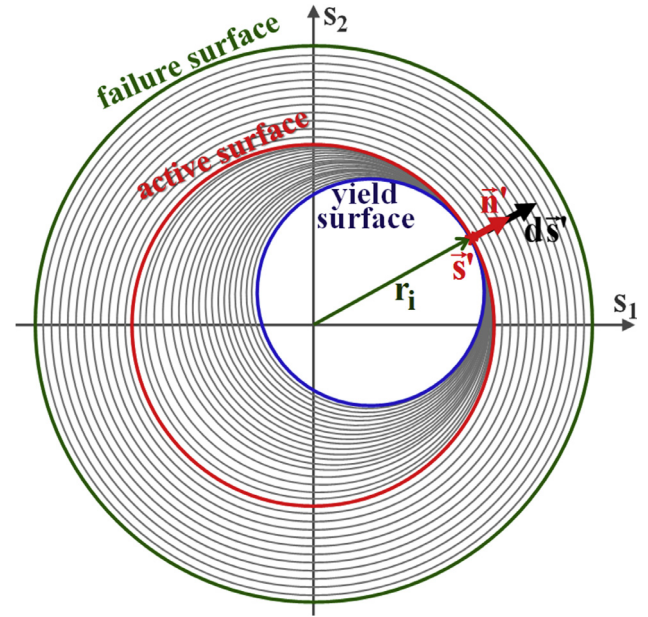


Fig. 5. Mróz infinite-surface hardening model for a monotonic proportional loading.

$$E^* \equiv E/[1 - \nu \cdot (\lambda_2 + \lambda_3)], \quad H_c^* \equiv H_c \cdot \frac{[1 - (\lambda_2 + \lambda_3) + (\lambda_2^2 + \lambda_3^2) - \lambda_2 \lambda_3]^{(h_c-1)/2}}{[1 - (\lambda_2 + \lambda_3)/2]^{h_c}} \quad (22)$$

$$\begin{cases} \varepsilon_{1el} = \sigma_1/E^*, \varepsilon_{1pl} = (\sigma_1/H_c^*)^{1/h_c}, \varepsilon_1 = \varepsilon_{1el} + \varepsilon_{1pl} \\ \sigma_2 = \lambda_2 \sigma_1, \sigma_3 = \lambda_3 \sigma_1 \\ \varepsilon_2 = \phi_{2el} \cdot \varepsilon_{1el} + \phi_{2pl} \cdot \varepsilon_{1pl}, \varepsilon_3 = \phi_{3el} \cdot \varepsilon_{1el} + \phi_{3pl} \cdot \varepsilon_{1pl} \end{cases} \quad (23)$$

$$\phi_{2pl} = \frac{\lambda_2 - 0.5 \cdot (1 + \lambda_3)}{1 - 0.5 \cdot (\lambda_2 + \lambda_3)}, \quad \phi_{3pl} = \frac{\lambda_3 - 0.5 \cdot (1 + \lambda_2)}{1 - 0.5 \cdot (\lambda_2 + \lambda_3)} \quad (24)$$

$$\phi_{2el} = \frac{\lambda_2 - \nu \cdot (1 + \lambda_3)}{1 - \nu \cdot (\lambda_2 + \lambda_3)}, \quad \phi_{3el} = \frac{\lambda_3 - \nu \cdot (1 + \lambda_2)}{1 - \nu \cdot (\lambda_2 + \lambda_3)} \quad (25)$$

Hence, Dowling's model for in-phase proportional loadings is a particular case of this more general in-phase proportional UNR, setting $\bar{\alpha}_U = 1$ (to reproduce Neuber's rule) and also $\lambda_3 = 0$ (free-surface with $\sigma_3 = 0$), assuming as well that $\phi_{2pl} = \phi_{2el}$ based on ν , and that $\phi_{3pl} = \phi_{3el}$ based on an effective Poisson ratio $\bar{\nu}$.

Both Dowling's and UNR multiaxial stress/strain concentration models assume the nominal section away from the notch remains LE. In other words, they are valid even under general yielding of the net cross section, but they do not account for gross yielding of the nominal cross section. To perform this correction, the pseudo principal stress $\bar{\sigma}_1$ is represented as the product of a LE stress concentration factor K_t multiplied by a nominal stress σ_{n1} , i.e. $\sigma_{n1} \equiv \bar{\sigma}_1/K_t$, where σ_{n1} is assumed to follow Ramberg-Osgood, giving

$$K_t^2 \cdot \sigma_{n1} \cdot \left[\frac{\sigma_{n1}}{E^*} + \bar{\alpha}_U \cdot \left(\frac{\sigma_{n1}}{H_c^*} \right)^{1/h_c} \right] = \sigma_1 \cdot \left[\frac{\sigma_1}{E^*} + \bar{\alpha}_U \cdot \left(\frac{\sigma_1}{H_c^*} \right)^{1/h_c} \right] \quad (26)$$

where the material parameters E^* and H_c^* defined by Eq. (22) consider the load multiaxiality, while the parameter $\bar{\alpha}_U$ considers local triaxial or rather transversal plasticity restrictions induced by the sharpness of the notch tip.

5. Verification of UNR predictions with elastoplastic finite elements

The proposed UNR and Dowling's classic notch rules are checked against elastoplastic (EP) Finite Element (FE) calculations, for multiaxial in-phase proportional tension-torsion problems. The comparison is based on the calculation of the peak EP stresses and strains at the tip of a notch in a solid shaft with largest diameter 50.8 mm and semi-circular U-notches with various tip radii. The shaft is assumed made of a heat-treated 1070 steel with Young modulus $E = 210$ GPa, Poisson ratio $\nu = 0.3$, and Ramberg-Osgood parameters $H_c = 1736$ MPa and $h_c = 0.199$, as reported in [23].

The quality of numerical results in FE models usually depends on the refinement of their mesh, whereas their computational cost is directly associated with the size of the numerical model. An excessively refined model may require too much memory or too long processing time. An efficient procedure to avoid these problems is to use submodeling techniques, which consist in adopting a very refined mesh only in a small part of the much less refined global model needed to describe the overall behavior of the component in question. This procedure is particularly useful when a denser refinement is necessary only in a specific region to be analyzed, such as near notch or crack tips. The submodeling technique involves two calculation steps: (a) solving the global model shown in Fig. 6, without considering a denser refinement in the region to be analyzed; and (b) solving the submodel with a much more refined mesh, which is loaded by prescribed displacements on its boundary obtained from the displacement field solution of the global model [36].

The goal of the submodels used in this work was to reduce the computational cost without compromising the accuracy of the EP

stress and strain distributions calculated around the notch tip. So, first a 3D non-linear finite element global model was generated in the ANSYS software, using 3D SOLID186 elements with 20 nodes each and 3 degrees of freedom per node. The loads were applied at one end of the specimen, with appropriate support conditions specified at the opposite end. The applied loads include pure tension, pure torsion, and multiaxial combinations of tension and torsion with three different proportionality stress ratios $R_{\tau\sigma}$, as described in detail in the following sections. After the solution of the global model, the submodel was generated using the same type of element. The small submodel boundary was placed far enough from the stress concentration region near the notch tip, and the load applied in its boundary was simulated by the displacement fields obtained from the solution of the global model, as illustrated in the scheme shown in Fig. 7.

The non-linearity of the material (1070 steel) was modeled by a Ramberg-Osgood stress-strain curve, considering a multilinear isotropic hardening model. Fig. 8 shows the stress-strain curve of this steel simulated by 97 equally distributed points. This figure also shows the adopted values of modulus of elasticity (E), Poisson's ratio (ν), and Ramberg-Osgood parameters (H_c and h_c), which describe the strain-hardening behavior of the material.

5.1. Convergence tests

Before analyzing the submodels used in this work, a mesh convergence study was performed to establish the mesh refinement parameters needed for the simulations. Such convergence tests were performed using the submodeling procedure described in the previous section in a LE model with a notch tip radius

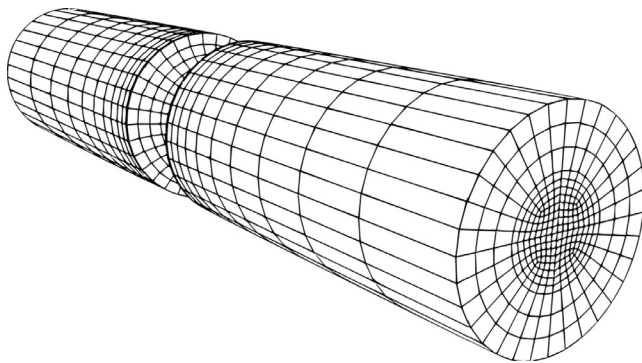


Fig. 6. Global model.

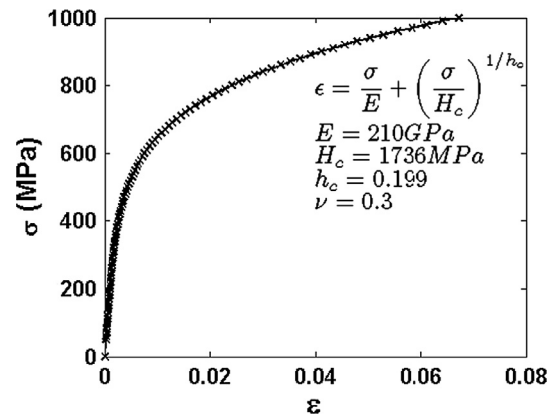


Fig. 8. Stress-strain curve of the 1070 steel.

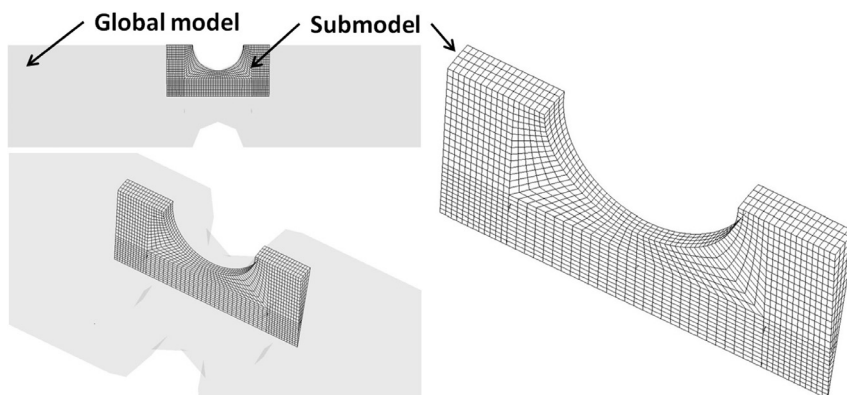


Fig. 7. Global model and submodel used in this work.

$\rho = 12.7$ mm subjected to a multiaxial load with proportionality stress ratio (torsion over tension) $R_{\tau\sigma} = 1.133$, in order to compare the calculations with available literature results [22]. Fig. 9 shows the submodel in the global model used for the convergence tests, indicating the location of its boundary surfaces. The minimum distance between the notch surface and the submodel boundary surfaces is set equal to the notch radius ρ .

In this 3D analysis, the submodel is a sector of the global model cylinder. So, the convergence tests need to verify as well an adequate value for the cylinder sector cutting angle θ , see Fig. 10. To verify the mesh size needed, the convergence study adopted a uniform mesh refinement, varying the number of elements along the notch surface from 4 up to 60 elements, and the submodel sector cutting angle from 10° to 90° . Some of the submodel meshes used this study are shown in Table 1.

Figs. 11 and 12 show typical results obtained from the mesh refinement convergence tests, plotting the stress values at points 1, 2, and 3 from Fig. 9 versus the ratio between the notch tip radius and the element size ρ/FE_s , for submodel sector angles $\theta = 10^\circ$ (Fig. 11) and $\theta = 70^\circ$ (Fig. 12). These results indicate that the normal σ_y and shear τ_{xy} stresses converge for $\rho/FE_s > 8$, independently of the submodel sector angle. However, the mean relative error between the normal stress observed at the submodel boundary and their corresponding region on the global model is 7.5% for a submodel sector angle $\theta = 10^\circ$ (Fig. 11), a value that drops to approximately 2.5% when the simulations are carried out using

$\theta = 70^\circ$ (Fig. 11). These results indicate that an adequate submodel sector angle θ should be verified for each notch geometry studied, a procedure used for the models analyzed in this work.

The normal σ_y and shear τ_{xy} stresses at the critical notch point converged for the $\theta = 70^\circ$ model to 416.4 MPa and 222.6 MPa, respectively, as shown in Table 2. These results confirmed the stress concentration factors for tension $K_{t\sigma} = 1.41$ and torsion $K_{t\tau} = 1.15$ reported by Köettgen et al. in [22], which are slightly different from those reported by Peterson [37], $K_{t\sigma} = 1.45$ and $K_{t\tau} = 1.18$.

5.2. Multiaxial non-linear FE analysis results

The following non-linear elastoplastic numerical simulations consider 3 models with different notch sizes, as listed in Table 3, which includes their LE stress concentration factors according to Peterson [37]. For each model, five proportional loadings are considered, varying the proportionality torsion/tension stress ratio: pure tension ($R_{\tau\sigma} = 0$), multiaxial loadings with 3 proportionality stress ratios ($R_{\tau\sigma} = \sqrt{3}/3$, $\sqrt{3}$, and $3\sqrt{3}$), and pure torsion ($R_{\tau\sigma} \rightarrow \infty$), as shown in Fig. 13.

The mesh refinement convergence study indicated that the ratio between the notch tip radius and the finite element size should be > 8 , and to obey this limit the mesh chosen for the models has $\rho/FE_s = 8.913$. A LE convergence study on the value of the submodel sector angle θ was performed as well for each notch

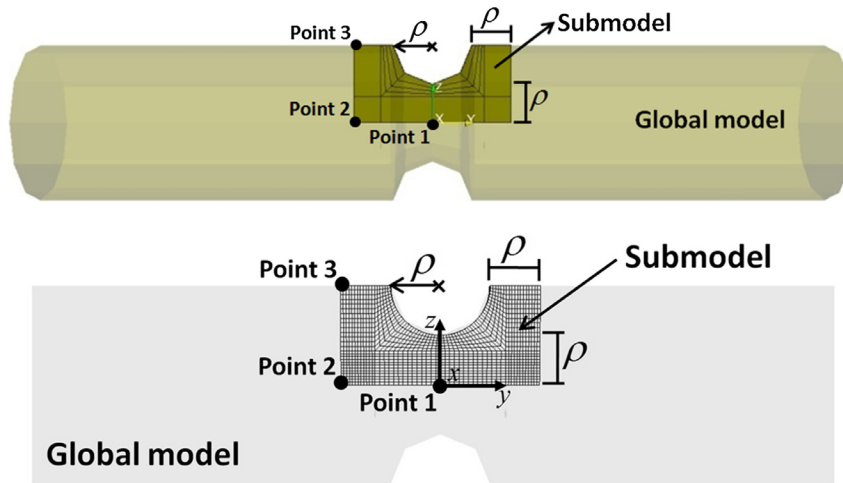


Fig. 9. Global model and submodel details.

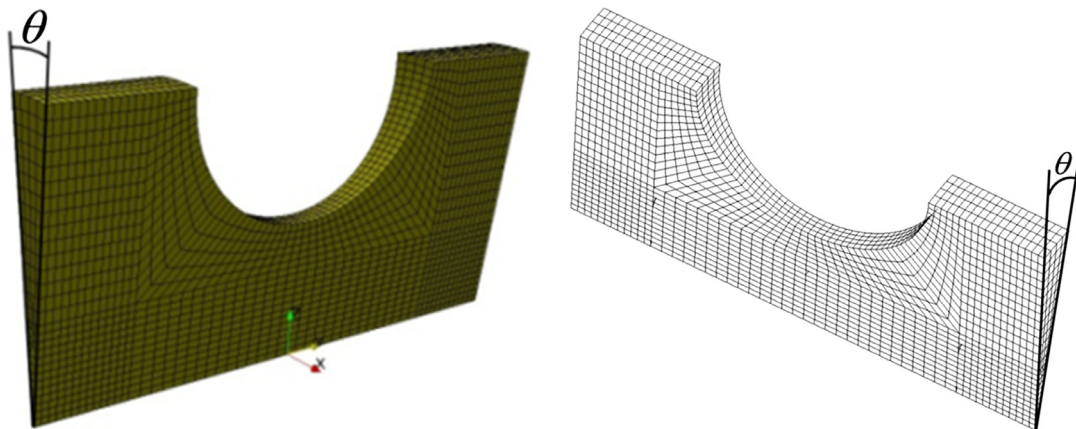


Fig. 10. The submodel as a sector of the global model cylinder.

Table 1
Mesh refinement of convergence tests.

# \ θ	10°	30°	50°	70°
4				
28				
60				

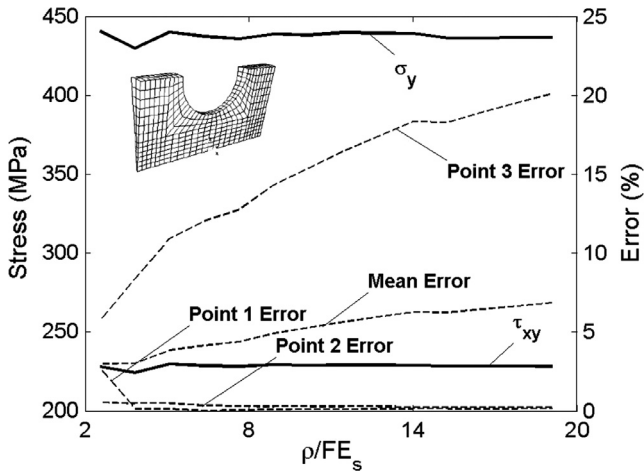


Fig. 11. Mesh refinement convergence results for $\theta = 10^\circ$.

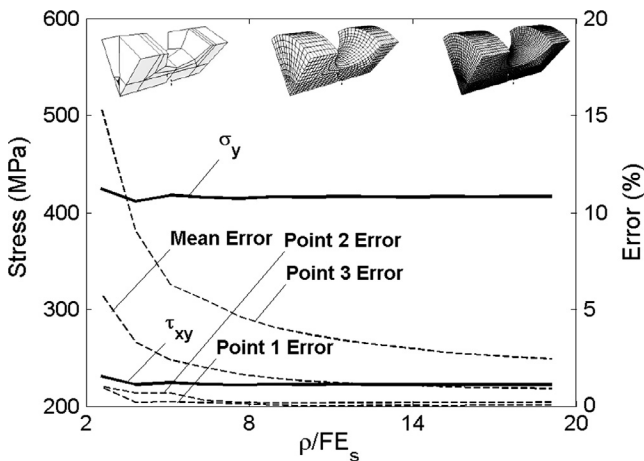


Fig. 12. Mesh refinement convergence results for $\theta = 70^\circ$.

Table 2
Stress concentration factors obtained from the convergence tests.

θ	σ [MPa]	$K_{t\sigma}$	τ [MPa]	$K_{t\tau}$
10°	438.7	1.49	229.0	1.19
30°	423.5	1.44	223.4	1.16
50°	418.6	1.42	222.9	1.15
70°	416.4	1.41	222.6	1.15
90°	415.3	1.41	222.2	1.15

Table 3
Modeled notches and their LE stress concentration factors according to Peterson [37].

ρ [mm]	Peterson	
	$K_{t\sigma}$	$K_{t\tau}$
2.54	2.65	1.57
0.762	4.10	2.30
0.254	6.70	3.75

The pseudo-stresses, which are the input data for the proposed UNR model, were calculated using the Ramberg-Osgood model for the material stress/strain behavior, which does not recognize a purely elastic response. However, using a low von Mises equivalent stress approximately equal to 100 MPa, the modeled steel has an essentially LE behavior at this stress level, see again its stress-strain curve shown in Fig. 8. So, these pseudo stresses $\bar{\sigma}_y$, $\bar{\sigma}_x$, and $\bar{\tau}_{xy}$ satisfied the LE hypothesis of the problem as expected, due to the linear behavior of the material under this low initial load. This is confirmed by comparing in Table 4 the calculated $K_{t\sigma}$ and $K_{t\tau}$ with the values reported by Peterson in [37]. However, it may be observed in Table 4 that the differences between stress concentration factors calculated by Peterson and by the present FE analysis are smaller for lower stress concentration factors. This could be caused by the non-linearity of the material at the notch root, which must have been triggered in the non-linear FE model, even for the lower initial load level.

The proposed UNR model depends on an adjustable parameter (α_U , see Eqs. (16) and (17)), which was calculated by minimizing the root mean square error (RMSe) between the normalized strains calculated by the UNR model ($\epsilon_{Mises}/\tilde{\epsilon}_{Mises})_{UNR}$ and the corresponding non-linear strains obtained from the FE model for each one of the n loads studied ($\epsilon_{Mises}/\tilde{\epsilon}_{Mises})_{FE}$, using

geometry studied, maintaining fixed the ρ/FE_s ratio. Based on it, $\theta = 30^\circ, 5^\circ$ and 2.5° were chosen to simulate notch tip radii $\rho = 2.54, 0.762$ and 0.254 mm, respectively.

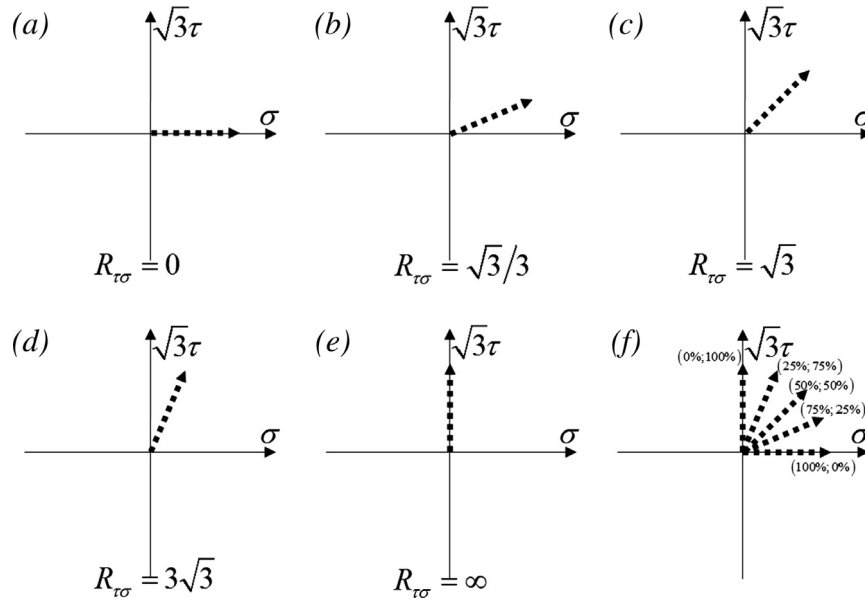


Fig. 13. Loading paths with different proportionality torsion/tension stress ratios $R_{\tau\sigma}$.

Table 4
Stress concentration factors calculated by Peterson and by the FE models.

ρ [mm]	Peterson		FEM	
	$K_{t\sigma}$	$K_{t\tau}$	$K_{t\sigma}$	$K_{t\tau}$
2.54	2.65	1.57	2.43	1.53
0.762	4.10	2.30	4.27	2.32
0.254	6.70	3.75	7.55	3.66

$$RMSe(\%) = 100 \cdot \sqrt{\sum_{i=1}^n [(\dot{\epsilon}_{Mises}/\dot{\tilde{\epsilon}}_{Mises})_{UNR} - (\dot{\epsilon}_{Mises}/\dot{\tilde{\epsilon}}_{Mises})_{FE}]^2/n} \quad (27)$$

Table 5 shows values of α_U calculated minimizing the RMSe of the normalized strains for the three notch tip radii and for the deviatoric version of the UNR model. It indicates that there is no clear trend on how the notch constraint factor α_U changes from pure tension ($R_{\tau\sigma} = 0$) to pure torsion ($R_{\tau\sigma} = \infty$), including the 3 different proportionality stress ratios ($R_{\tau\sigma} = \sqrt{3}/3$, $\sqrt{3}$, and $3\sqrt{3}$), when adjusting it for each load type and notch geometry. For the two sharper notches, the model yielded smaller RMSe values minimized for both the normalized strain ($\dot{\epsilon}_{Mises}/\dot{\tilde{\epsilon}}_{Mises}$) and stress

Table 5
 α_U and their respective RMSe (%) minimized for each load ratio $R_{\tau\sigma}$.

$K_{t\sigma}$	$K_{t\tau}$	ρ [mm]	$R_{\tau\sigma}$	α_U	Deviatoric UNR	
					$\dot{\epsilon}_{Mises}/\dot{\tilde{\epsilon}}_{Mises}$	$\sigma_{Mises}/\tilde{\sigma}_{Mises}$
2.43	1.53	2.54	0	1.476	1.56	1.03
			$\sqrt{3}/3$	1.451	1.81	1.01
			$\sqrt{3}$	1.127	4.20	1.05
			$3\sqrt{3}$	0.717	7.52	1.43
			∞	0.515	10.31	1.72
4.27	2.32	0.762	0	1.692	0.47	1.13
			$\sqrt{3}/3$	1.719	0.52	1.11
			$\sqrt{3}$	1.708	1.03	1.06
			$3\sqrt{3}$	1.452	2.29	0.98
			∞	1.233	3.29	0.99
7.55	3.66	0.254	0	1.707	0.18	1.17
			$\sqrt{3}/3$	1.773	0.14	1.18
			$\sqrt{3}$	1.979	0.17	1.21
			$3\sqrt{3}$	2.060	0.12	1.20
			∞	1.904	0.34	1.17

($\sigma_{Mises}/\tilde{\sigma}_{Mises}$) curves calculated by the deviatoric UNR model. So, it can be argued that the proposed parameter α_U is almost independent of the applied load.

For the deviatoric UNR model, there is a range of α_U values that decreases when the notch becomes sharper for all load types, namely $\alpha_U = 0.515$ – 1.476 , 1.233 – 1.719 and 1.707 – 2.060 for the three notch geometries. Assuming a constant α_U value for a given notch, achieved by minimizing the RMSe (%) for all 5 types of loads, the results of this overall α_U calculation are summarized in Table 6, which resumes all the calculated values. Considering the UNR model in its deviatoric version, these constant α_U values are 0.989, 1.549, and 1.874 for the notches with $K_{t\sigma} = 2.43$, 4.27, and 7.55, respectively, while for the UNR non-deviatoric model the corresponding α_U values are 1.218, 1.864, and 2.239. As shown in Fig. 14, it was also observed that, like Newman’s constraint factor α for crack tips [34], α_U changes monotonically for the different notch geometries. After fitting α_U for each notch geometry, the RMSe values are calculated for each load type described by its $R_{\tau\sigma}$ between the normalized strain ($\dot{\epsilon}_{Mises}/\dot{\tilde{\epsilon}}_{Mises}$) and stress ($\sigma_{Mises}/\tilde{\sigma}_{Mises}$) curves proposed by the UNR model, as indicated in Table 7.

The proposed UNR model was compared with the traditional Neuber [4] and Molski-Glinka [8] models, using both their deviatoric and non-deviatoric versions, as also shown in Tables 6 and 7. It may be observed that Neuber’s model ($\alpha_U = 1$) yielded better results in its deviatoric version, when compared to its much more commonly used non-deviatoric formulation. On the other hand, Molski-Glinka’s ($\alpha_U = 2$) non-deviatoric version showed better results for the blunt notch when compared to its deviatoric version, but its predictions worsen as the notch becomes sharper. However, in its deviatoric version, the sharper notch geometries present smaller errors. Thus, these results justify the use of Neuber and/or Molski-Glinka models in their deviatoric versions. This observation confirms the opinion expressed by Kujawski in [33], who stated that Neuber’s rule in terms of deviatoric energy has a coherent formulation for multiaxial loading conditions, including uniaxial tension and pure shear. However, the correlation for general multiaxial stress states needs to be further investigated.

Figs. 15–17 illustrate the main results obtained for each notch type by plotting the deviatoric UNR and the classic non-deviatoric Neuber and Molski-Glinka predictions, as well as the

Table 6
 α_U and RMSe (%) minimized for all 5 load types with varying $R_{\tau\sigma}$.

$K_{t\sigma}$	$K_{t\tau}$	ρ [mm]	$R_{\tau\sigma}$	α_U	Deviatoric UNR		Non-deviatoric UNR		α_U	Deviatoric Neuber		Non-deviatoric Neuber		α_U	Deviatoric Glinka		Non-deviatoric Glinka	
					$\epsilon_{Mises}/\epsilon_{Mises}$	$\sigma_{Mises}/\sigma_{Mises}$	$\epsilon_{Mises}/\epsilon_{Mises}$	$\sigma_{Mises}/\sigma_{Mises}$		$\epsilon_{Mises}/\epsilon_{Mises}$	$\sigma_{Mises}/\sigma_{Mises}$	$\epsilon_{Mises}/\epsilon_{Mises}$	$\sigma_{Mises}/\sigma_{Mises}$		$\epsilon_{Mises}/\epsilon_{Mises}$	$\sigma_{Mises}/\sigma_{Mises}$	$\epsilon_{Mises}/\epsilon_{Mises}$	$\sigma_{Mises}/\sigma_{Mises}$
2.43	1.53	2.540	0–	0.989	12.73	1.81	1.218	12.73	1	12.73	1.83	13.95	1.79	2	22.60	4.33	18.90	3.47
4.27	2.32	0.762	∞	1.549	4.00	1.17	1.864	12.54	1.29	12.54	1.29	18.37	2.16	7.81	2.41	4.45	4.45	1.50
7.55	3.66	0.254		1.874	1.81	1.22	2.239	17.08	1.97	17.08	1.97	23.12	2.90	2.48	1.56	3.57	3.57	0.65

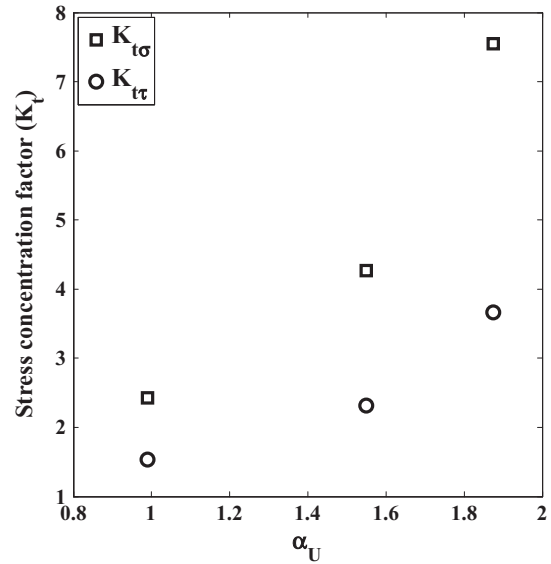


Fig. 14. α_U values for the different notch geometries.

results obtained from the non-linear FE model calculations, for $R_{\tau\sigma} = \sqrt{3}$. For the blunter notch shown in Fig. 15, the overall $\alpha_U = 0.989$ fitting for all load types generated a minimized RMSe = 12.73% between its strain predictions and the FE calculations, and a RMSe = 1.81% between its stress predictions and the FE results. Likewise, the equivalent errors for Neuber are 13.95% and 1.79%, whereas for Molski-Glinka they are 18.90% and 3.47%, see Table 6. The same trend was observed as the notch becomes sharper, see Figs. 16 and 17.

Furthermore, it was also observed that the UNR model has the versatility to interpolate between the classic Neuber and Molski-Glinka models depending on the notch severity, as observed for the notches with $K_{t\sigma} = 2.43$ and 4.27, see Figs. 15 and 16, or even to extrapolate them for very sharp notches, such as the one with $K_{t\sigma} = 7.55$, see Fig. 17.

Note in Figs. 16 and 17 that, even though the errors in the predicted notch-root stresses are not high for the several studied models, the errors in strain can be very significant, in special when the strain-life non-linearity is also considered in fatigue life calculations. For instance, Glinka's original (non-deviatoric) rule predicts reasonably well both notch-root stresses and strains in Fig. 16, but it significantly overestimates strains for the higher constraint case from Fig. 17, which could result in fatigue life errors of an order of magnitude. The main advantage of the proposed UNR is to allow the calibration of the constraint effect through α_U to reduce such errors.

Note also that the submodeling technique would not be appropriate under very high elastoplastic nominal stresses, since geometric non-linearities would have impacts on the finite element results. To evaluate the influence of geometric nonlinearities induced by the loads used to simulate high elastoplastic nominal stresses at the notch root, the final radius of the plastically deformed notch was computed. For the multiaxial case with $R_{\tau\sigma} = -\sqrt{3}$, $\rho = 0.254$ mm and under the highest simulated loading, the notch radius ρ only increased by 0.059% (to $\rho = 0.2555$ mm) in the elastoplastic simulations. This deformed geometry was then simulated again using a linear elastic FE analysis to evaluate the shift in the linear elastic stress concentration factors $K_{t\sigma}$ and $K_{t\tau}$ due to geometric distortions, resulting in 7.53 and 3.65, respectively, corresponding to a reduction of less than 0.3% of both fac-

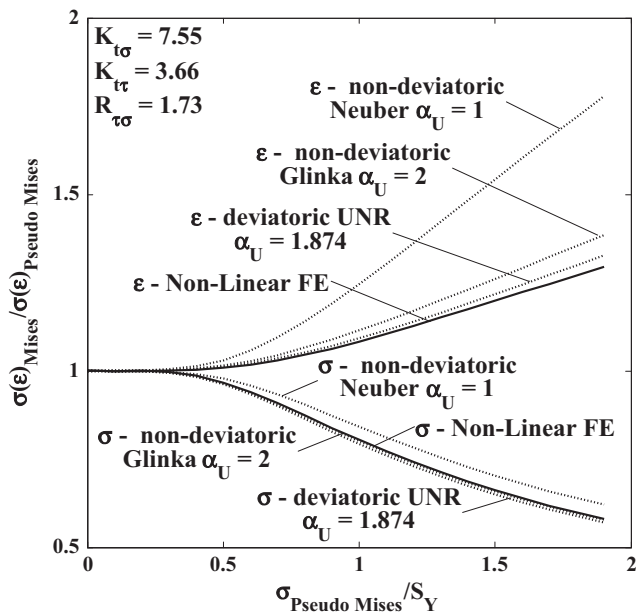


Fig. 17. Deviatoric UNR, non-deviatoric Neuber and Molski-Glinka, and nonlinear finite element stress concentration predictions for $K_{\tau\sigma} = 7.55$ and $R_{\tau\sigma} = \sqrt{3}$.

even in cases where it is not possible or desirable to make simplified EP stress/strain concentration predictions using the UNR model, the FE calculations indicate that it is highly recommended to use the Neuber and Molski-Glinka models in their deviatoric versions, instead of using them in their more common/classic non-deviatoric versions.

6. Conclusions

In this work, a Unified Notch Rule (UNR) is proposed and extended to multiaxial proportional loading histories. Moreover, it is validated by comparing its predictions with elastoplastic Finite Element calculations on notched shafts, both for uniaxial and for in-phase proportional multiaxial loading histories. The UNR can reproduce Neuber's or Molski-Glinka's rules, and interpolate their notch-tip behaviors through an adjustable parameter α_U , an way to consider increasing plasticity restrictions cause by transversal constraints at the notch tip as their stress concentration factor increases, such as proposed by Newman for crack tips. It was found that the UNR model can better estimate strains and stresses at notch tips than the traditional Neuber and Molski-Glinka models, as studied for the pure tension, pure torsion and combined tension-torsion loadings. Moreover, it is found that if for any reason it is not possible or desirable to estimate multiaxial elastoplastic stress/strain concentration effects using the UNR model instead of traditional Neuber and Molski-Glinka models, it is then recommendable to use such models in their deviatoric versions.

References

- [1] Socie DF, Marquis GB. *Multiaxial fatigue*. SAE; 2000.
- [2] Castro JTP, Meggiolaro MA. *Fatigue Design Techniques, vol. 2: Low-Cycle and Multiaxial Fatigue*. ISBN 1530797047, CreateSpace; 2016.
- [3] Meggiolaro MA, Castro JTP. Automation of the fatigue design under variable amplitude loading using the ViDa software. *Int J Struct Integrity* 2010;1:1–6.
- [4] Neuber H. Theory of stress concentration for shear-strained prismatical bodies with an arbitrary non-linear stress-strain law. *J. Appl Mech* 1961;28:544–51.
- [5] Topper TH, Wetzell RM, Morrow JD. Neuber's rule applied to fatigue of notched specimens. *J Mater* 1969;1:200–9.

- [6] Harkergard G, Mann T. Neuber prediction of elastoplastic strain concentration in notched tensile specimens under large range yielding. *J Strain Anal* 2003;38:79–94.
- [7] Sonsino CM. Zur bewertung des schwingfestigkeitsverhaltens von bauteilen mit hilfe örtlicher beanspruchungen. *Sonderdruck aus Konstruktion* 1993;45 (H1):S25–33.
- [8] Molski K, Glinka G. A method of elastoplastic and strain calculation at a notch root. *Mater Sci Eng* 1981;50:93–100.
- [9] Meggiolaro MA, Castro JTP, Góes RCO. Elastoplastic nominal stress effects in the estimation of the notch-tip behavior in tension. *Theor App Fract Mech* 2016;84:86–92.
- [10] Stephens RI, Fatemi A, Stephens RR, Fuchs HO. *Metal fatigue in engineering*. 2nd ed. Interscience; 2000.
- [11] Durán JAR, Castro JTP, Payão Filho JC. Fatigue crack propagation prediction by cyclic plasticity damage accumulation models. *Fatigue Fract Eng Mater Struct* 2003;26(2):137–50.
- [12] Castro JTP, Meggiolaro MA, Miranda ACO. Singular and non-singular approaches for predicting fatigue crack growth behavior. *Int J Fatigue* 2005;27:1366–88.
- [13] Meggiolaro MA, Castro JTP. Statistical evaluation of strain-life fatigue crack initiation predictions. *Int J Fatigue* 2004;26:463–76.
- [14] Martin JF, Topper TH, Sinclair GM. Computer based simulation of cyclic stress-strain behavior with applications to fatigue. *Mater Res Standards* 1971;11:23–8.
- [15] Amzallag C, Gerey JP, Robert JL, Bahuau J. Standardization of the rainflow counting method for fatigue analysis. *Int J Fatigue* 1994;16:287–93.
- [16] McInnes CH, Meehan PA. Equivalence of four-point and three-point rainflow cycle counting algorithms. *Int J Fatigue* 2008;30:547–59.
- [17] Williams DP, Topper TH. A generalized model of structural reversed plasticity. *Exp Mech* 1981;21:145–54.
- [18] Chaboche JL. A review of some plasticity and viscoplasticity constitutive theories. *Int J Plasticity* 2008;24:1642–93.
- [19] Meggiolaro MA, Wu H, Castro JTP. Non-proportional hardening models for predicting mean stress relaxation and multiaxial ratcheting in fatigue problems - Part I: Ilyushin spaces. *Int J Fatigue* 2016;82:146–57.
- [20] Meggiolaro MA, Castro JTP, Wu H. A general class of non-linear kinematic models to predict mean stress relaxation and multiaxial ratcheting in fatigue problems - Part I: Ilyushin spaces. *Int J Fatigue* 2016;82:158–66.
- [21] Meggiolaro MA, Castro JTP, Wu H. A general class of non-linear kinematic models to predict mean stress relaxation and multiaxial ratcheting in fatigue problems - Part II: Generalized surface translation rule. *Int J Fatigue* 2016;82:167–78.
- [22] Köettgen VB, Barkey ME, Socie DF. Pseudo stress and pseudo strain based approaches to multiaxial notch analysis. *Fatigue Fract Eng Mater Struct* 1995;18:981–1006.
- [23] Köettgen VB, Barkey ME, Socie DF. Pseudo stress and pseudo strain based approaches to multiaxial notch analysis. *Fracture Control Program Report #169, U Illinois at Urbana-Champaign*; 1995.
- [24] Hoffmann M, Seeger T. A generalized method for estimating multiaxial elastic-plastic notch stresses and strains, part 1: theory. *J Eng Mater Technol* 1985;107:250–4.
- [25] Hoffmann M, Seeger T. A generalized method for estimating multiaxial elastic-plastic notch stresses and strains, part 2: application and general discussion. *J Eng Mater Technol* 1985;107:255–60.
- [26] Dowling NE, Brose WR, Wilson WK. Notched member fatigue life predictions by the local strain approach. In: *Fatigue under complex loading: analysis and experiments*, AE-6, SAE; 1977.
- [27] Salemi Z, Kujawski D. A strain energy method for elastic-plastic analysis of notches under shear loading. *Theor App Fract Mech* 2016;84:49–56.
- [28] Ince A. Numerical validation of elasto-plastic stress and strain analysis model for notched components subject to non-proportional loadings. *Theor App Fract Mech* 2016;84:26–37.
- [29] Marangon C, Campagnolo A, Berto F. Three-dimensional effects at the tip of rounded notches subjected to mode-I loading under cyclic plasticity. *J Strain Anal Eng Des* 2015;50:299–313.
- [30] Ye D, Hertel O, Vormwald M. A unified expression of elastic-plastic notch stress-strain calculation in bodies subjected to multiaxial cyclic loading. *Int J Solids Struct* 2008;45:6177–89.
- [31] Ince A, Glinka G. A numerical method for elasto-plastic notch-root stress-strain analysis. *J Strain Analysis Eng Design* 2013;48:229–44.
- [32] Ince A, Glinka G. Innovative computational modeling of multiaxial fatigue analysis for notched components. *Int J Fatigue* 2016;82:134–45.
- [33] Kujawski D. On energy interpretations of the Neuber's rule. *Theor Appl Fract Mech* 2014;73:91–6.
- [34] Newman JC, Crews JH, Bigelow CA, Dawicke DS. Variations of the global constraint factor in cracked bodies under tension and bending loads. *ASTM STP* 1244:21–42; 1995.
- [35] Chu CC. The analysis of multiaxial cyclic problems with an anisotropic hardening model. *Int J Solids Struct* 1987;23:567–79.
- [36] ANSYS 12.1 help//Mechanical APDL (formerly ANSYS)//Advanced analysis techniques guide//9. Sub modeling.
- [37] Pilkey WD. *Peterson's stress concentration factors*. 2nd ed. Wiley; 1997.